J|A|C|S ARTICLES

Published on Web 02/18/2010

Toward Structural Dynamics: Protein Motions Viewed by Chemical Shift Modulations and Direct Detection of C′N Multiple-Quantum Relaxation

Mirko Mori,[†] Fatiha Kateb,[‡,||] Geoffrey Bodenhausen,[‡,§] Mario Piccioli,[†] and Daniel Abergel*[,‡]

Magnetic Resonance Center (CERM) and Department of Chemistry, University of Florence, Via L. Sacconi 3, 50019 Sesto Fiorentino, Italy, Laboratoire des Biomolécules, associé au CNRS, Département de Chimie, Ecole Normale Supérieure, 24, rue Lhomond, 75231 Paris cedex 05, France, and Institut des Sciences et Ingénierie Chimiques, Ecole Polytechnique Fédérale de Lausanne, Batochime, 1015 Lausanne, Switzerland

Received December 8, 2009; E-mail: daniel.abergel@ens.fr

Abstract: Multiple quantum relaxation in proteins reveals unexpected relationships between correlated or anti-correlated conformational backbone dynamics in α-helices or β-sheets. The contributions of conformational exchange to the relaxation rates of C′N coherences (i.e., double- and zero-quantum coherences involving backbone carbonyl $^{13}C'$ and neighboring amide ^{15}N nuclei) depend on the kinetics of slow exchange processes, as well as on the populations of the conformations and chemical shift differences of $^{13}C'$ and ^{15}N nuclei. The relaxation rates of C′N coherences, which reflect concerted fluctuations due to slow chemical shift modulations (CSMs), were determined by direct ^{13}C detection in diamagnetic and paramagnetic proteins. In well-folded proteins such as lanthanide-substituted calbindin (CaLnCb), copper,zinc superoxide dismutase (Cu,Zn SOD), and matrix metalloproteinase (MMP12), slow conformational exchange occurs along the entire backbone. Our observations demonstrate that relaxation rates of C′N coherences arising from slow backbone dynamics have positive signs (characteristic of correlated fluctuations) in β-sheets and negative signs (characteristic of anti-correlated fluctuations) in α-helices. This extends the prospects of structure−dynamics relationships to slow time scales that are relevant for protein function and enzymatic activity.

Introduction

In recent years, there has been growing evidence that structural flexibility plays a key role for protein function. Many biochemical events such as enzymatic reactions, the formation or disruption of hydrogen bonds, the alteration of dihedral angles, and the reorientation of aromatic rings occur on slow micro- to millisecond time scales. The functional relevance of protein dynamics has been amply demonstrated, and its study by NMR has been one of our main goals. Beyond the celebrated structure−function relationships, several groups have proposed to investigate the existence of structure−dynamics relationships. We like to refer to "structural dynamics" in this context, since the expression "structural biology" has an unduly static connotation. Several empirical and theoretical attempts have been made to relate experimental observations of protein dynamics to molecular structure. In most studies, internal mobility is described in terms of rapid fluctuations about an average structure. These fluctuations are often modeled using local harmonic potentials, as in Normal Mode Analysis (NMA),[1] Gaussian Network Models (GNM),[2] Networks of Coupled Rotators (NCR),[3] and other methods. These approaches are mostly relevant to describe fast (subnanosecond) internal dynamics as reflected in relaxation rates (R_1, R_2, and Overhauser effects) of isolated ^{15}N or ^{13}C nuclei, although quantities such as order parameters and conformational entropy are not associated with any specific time scale of internal dynamics.

The situation is clearly different for conformational exchange, where NMR can provide insight into slow processes that occur in a microsecond to millisecond range. The contributions of conformational exchange processes to relaxation rates reflect the kinetic rate, populations, and chemical shifts of the nuclei in these conformations. Therefore, there is no simple relationship between NMR relaxation rates due to conformational exchange and protein structure, even if there may be some correlations between relaxation rates and various structural motifs such as α-helices and β-sheets. Structural fluctuations in the protein backbone may lead to chemical shift modulations (CSMs), the magnitudes and signs of which are not easy to predict.

In this work, these fundamental questions are addressed for a few well-structured proteins with different folds. Slow backbone fluctuations were studied by measuring isotropic CSMs of carbonyl/amide C′N coherences, using both novel direct ^{13}C detection and known indirect ^{1}H detection techniques. Direct ^{13}C detection ("protonless") experiments are to be preferred when ^{1}H signals suffer from (possibly paramagnetic)

[†] University of Florence.
[‡] Ecole Normale Supérieure.
[§] Ecole Polytechnique Fédérale de Lausanne.
[||] Present address: Lehrstuhl für Biomolekulare NMR-Spektroskopie, Departement Chemie, Lichtenbergstr. 4, D-85747 Garching, Germany.

(1) Levitt, M.; Sander, C.; Stern, P. *J. Mol. Biol.* **1985**, *181*, 423–447.
(2) Halioglu, T.; Bahar, I. *Proteins* **1999**, *37*, 654–667.
(3) Abergel, D.; Bodenhausen, G. *J. Chem. Phys.* **2005**, *123*, 204901.

10.1021/ja9103556

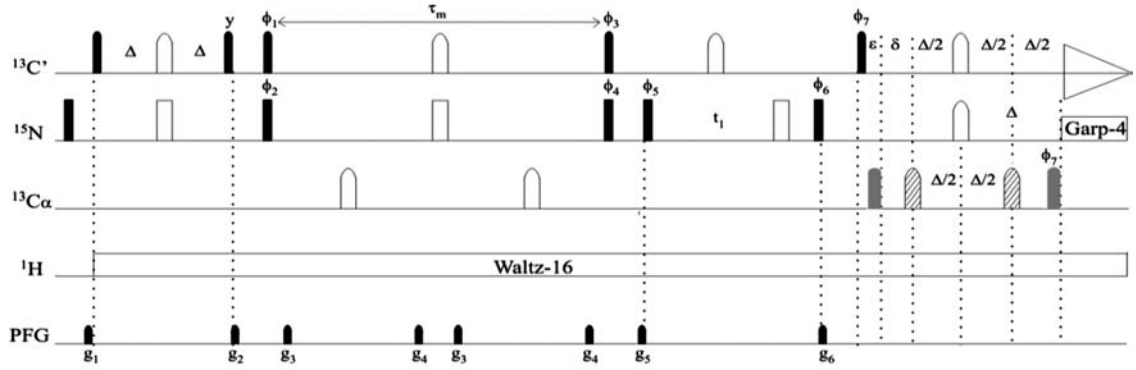

Figure 1. Pulse sequence designed to measure relaxation rates of $^{13}C'$-^{15}N multiple-quantum coherences. Pulses are applied along *x* unless otherwise indicated. Black and white pulses applied to the ^{15}N spins indicate nonselective 90° and 180° pulses. All ^{13}C pulses were band-selective; Q5 (or time-reversed Q5) shaped 90° ^{13}C pulses were used with durations of 256 μs. For $^{13}C^{\alpha}$ inversion pulses, Q3 shaped pulses were used with durations of 220 μs. The ^{13}C, ^{15}N, and ^{1}H carrier frequencies were centered at 173, 116, and 3.5 ppm, respectively. ^{1}H decoupling was performed with a 2.9 kHz WALTZ-16 sequence, and ^{15}N decoupling during acquisition was performed using a 2.9 kHz GARP-4 sequence. To suppress $J(C'C^{\alpha})$ couplings during acquisition, the in-phase (IP) and anti-phase (AP) components were acquired and stored separately. Pulses depicted in gray were used to acquire anti-phase components, while pulses represented by hatched shapes were used to obtain in-phase components.[12] The delays Δ, δ, and ε were set to 12.5, 1.75, and 4.5 ms, respectively. The mixing times were $\tau_m = 20$ and 40 ms. The durations of all sine-shaped gradients were 1 ms, and the peak amplitudes were $g_{1z} = 57$, $g_{2z} = 37$, $g_{3z} = -29$, $g_{4z} = -17$, $g_{5z} = 19$, and $g_{6z} = 41$ G cm^{-1}. The phases for the autorelaxation experiment were $\phi_1 = y, -y$; $\phi_2 = y, y, -y, -y$; $\phi_3 = 16\ y, 16\ -y$; $\phi_4 = 4\ y, 4\ -y$;$\phi_5 = 8\ x, 8\ -x$; $\phi_6 = 32\ x, 32\ -x$; $\phi_7 = x$ for in-phase acquisition, $\phi_7 = -y$ for anti-phase acquisition; $\phi_{rec} = (x, -x, -x, x, -x, x, x, -x)$, $2(-x, x, x, -x, x, -x, -x, x)$, $(x, -x, -x, x, -x, x, x, -x)$, $(-x, x, x, -x, x, -x, -x, x)$, $2(x, -x, -x, x, -x, x, x, -x)$, $(-x, x, x, -x, x, -x, -x, x)$. The phases for the cross-relaxation experiment were $\phi_1 = y, -y$; $\phi_2 = y, y, -y, -y$; $\phi_3 = 16\ x, 16\ -x$; $\phi_4 = 4\ x, 4\ -x$; $\phi_5 = 8\ x, 8\ -x$; $\phi_6 = 32\ x, 32\ -x$; $\phi_7 = x$ for in-phase acquisition; $\phi_7 = -y$ for anti-phase acquisition; $\phi_{rec} = (x, -x, -x, x, -x, x, x, -x)$, $2(-x, x, x, -x, x, -x, -x, x)$, $(x, -x, -x, x, -x, x, x, -x)$, $(-x, x, x, -x, x, -x, -x, x)$, $2(x, -x, -x, x, -x, x, x, -x)$, $(-x, x, x, -x, x, -x, -x, x)$.

line-broadening.[4,5] Even observables involving protons, such as H^NN or $H^{\alpha}C^{\alpha}$ residual dipolar couplings (RDCs), can be obtained using pulse sequences without detecting or exciting the protons directly.[6] Here, we extend the protonless methodology to dynamic studies. Direct detection of ^{13}C nuclei offers an alternative route to the measurement of relaxation rates of C′N multiple-quantum coherences,[7−9] which may contribute to a more complete description of backbone dynamics in proteins[10] as a complementary tool to conventional techniques that focus on the relaxation of isolated ^{15}N and ^{13}C nuclei.[11] Protonless experiments avoid losses of information caused by fast relaxation or exchange broadening of ^{1}H signals and may therefore offer better sensitivity, particularly in the presence of paramagnetic ions.

The observations presented in this work demonstrate that conformational exchange is not restricted to some regions of the backbone; rather, it is a phenomenon that extends across the entire backbone of structured proteins. Moreover, these results allowed us to discover a surprisingly simple correlation between the *type of secondary structure* (α-helix or *β*-sheet) and the *sign* of the CSM contributions, which is negative in α-helices and positive in *β*-sheets. These observations represent a significant step in understanding structure/dynamics relationships. A tentative rationalization will be proposed, based on published theoretical analyses.

Experimental Section

Sample Preparation. Protein expression and purification of native, Ca^{2+} loaded calbindin D_{9k} (Ca_2Cb), was performed as described elsewhere.[12] Lanthanide (Ln^{3+})-substituted derivatives (CaLaCb and CaCeCb) were obtained following the established procedure.[13] Sample concentrations were between 0.6 and 0.9 mM. Uniformly ^{13}C,^{15}N-labeled copper(I),zinc(II) superoxide dismutase was prepared and purified as described elsewhere.[14] The protein was concentrated to 1.0 mM, and reduction was achieved by addition of a 0.10 M solution of sodium isoascorbate in phosphate buffer at pH 6.0. The catalytic domain of MMP12, corresponding to the segment Gly-106−Gly-263, was cloned and expressed as reported in the literature.[13] After refolding, the catalytic domain was inhibited by *N*-isobutyl-*N*-[4-methoxyphenylsulphonyl] glycyl hydroxamic acid (NNGH). The 0.9 mM sample of ^{13}C,^{15}N-labeled MMP12 had a pH adjusted to 7.2.

NMR Experiments. All experiments were carried out on a Bruker Avance 700 MHz spectrometer at 298 K. Proton-detected experiments were performed with a standard inverse-detection, triple-resonance probe (TXI), and a customized triple-resonance probe with a ^{13}C-selective inner coil was used for ^{13}C-detected experiments. Protonless CON-type multiple-quantum experiments were performed using the pulse sequence shown in Figure 1. The 2D matrices consisted of 1024 and 128 points in the t_2 and t_1 dimensions. To determine auto- and cross-correlated relaxation rates, 128 and 512 scans were accumulated, respectively, with a 1.3 s relaxation delay. HNCO-type spectra were recorded using an

(4) Bertini, I.; Duma, L.; Felli, I. C.; Fey, M.; Luchinat, C.; Pierattelli, R.; Vasos, P. R. *Angew. Chem., Int. Ed.* **2004**, *43*, 2257–2259.
(5) Bermel, W.; Bertini, I.; Felli, I. C.; Piccioli, M.; Pierattelli, R. *Progr. NMR Spectrosc.* **2006**, *48*, 25–45.
(6) Balayssac, S.; Bertini, I.; Luchinat, C.; Parigi, G.; Piccioli, M. *J. Am. Chem. Soc.* **2006**, *128*, 15042–15043.
(7) Frueh, D.; Tolman, J. R.; Bodenhausen, G.; Zwahlen, C. *J. Am. Chem. Soc.* **2001**, *123*, 4810.
(8) Pellechia, M.; Pang, Y.; Wang, L.; Kurochkin, A. V.; Kumar, A.; Zuiderweg, E. R. P. *J. Am. Chem. Soc.* **1999**, *121*, 9165–9170.
(9) Majumdar, A.; Ghose, R. *J. Biomol. NMR* **2004**, *28*, 213–227.
(10) Kateb, F.; Abergel, D.; Blouquit, Y.; Duchambon, P.; Craescu, C. T.; Bodenhausen, G. *Biochemistry* **2006**, *45*, 15011–15019.
(11) Kordel, J.; Skelton, N. J.; Akke, M.; Palmer, A. G., III; Chazin, W. J. *Biochemistry* **1992**, *31*, 4856–4866.
(12) Chazin, W. J.; Kördel, J.; Drakenberg, T.; Thulin, E.; Brodin, P.; Grundstrom, T.; Forsén, S. *Proc. Natl. Acad. Sci. U.S.A.* **1989**, *86*, 2195–2198.
(13) Allegrozzi, M.; Bertini, I.; Janik, M. B. L.; Lee, Y.-M.; Liu, G.; Luchinat, C. *J. Am. Chem. Soc.* **2000**, *122*, 4154–4161.
(14) Mori, M.; Jiménez, B.; Piccioli, M.; Battistoni, A.; Sette, M. *Biochemistry* **2008**, *47*, 12954–12963.
(15) Banci, L.; Bertini, I.; Ciulli, A.; Fragai, M.; Luchinat, C.,; Terni, B. *J. Mol. Catal. A: Chem.* **2003**, *204−205*, 401–408.

established pulse sequence,[16] with 80 and 320 scans to reveal auto- and cross-peaks, respectively. Data processing was performed using the TOPSPIN software.

Analysis of $R^{CSM/CSM}$ Relaxation Rates. The mean and standard deviation of the ΔR rates were calculated for the complete set of data for each system following a procedure described elsewhere.[10] Outliers, defined as rates that lie farther that 1.5 standard deviations from the mean, were excluded. Trimmed averages and standard deviations were calculated for the remaining data. Rates were considered to be significantly different from the average if $R^{CSM/CSM} - \delta R^{CSM/CSM}$ was larger than $\langle R^{CSM/CSM}\rangle + \sigma$, or if $R^{CSM/CSM} + \delta R^{CSM/CSM}$ was smaller than $\langle R^{CSM/CSM}\rangle - \sigma$ (where $\delta R^{CSM/CSM}$ is the experimental error).

Pulse Sequences. The pulse sequence used to measure multiple-quantum relaxation rates via direct detection of C′ nuclei is shown in Figure 1. This sequence is a modified version of a CON experiment[17] where C′ coherence is converted via an INEPT-type building block into longitudinal two-spin order C'_zN_z. After a purging field gradient pulse, a coherence C'_xN_x is created by two simultaneous 90° pulses. This corresponds to a superposition of zero- and double-quantum terms:

$$2C'_xN_x = (C'_+N_- + C'_-N_+) + (C'_+N_+ + C'_-N_-) \quad (1)$$

The C'_xN_x coherence decays and is partly converted into C'_yN_y coherence during the mixing time τ_m, which can be expressed in terms of zero- and double-quantum relaxation rates R_{DQ} and R_{ZQ}:

$$\begin{aligned}2C'_xN_x \rightarrow\ & C'_xN_x[\exp(-R_{ZQ}\tau_m)(C'_+N_- + C'_-N_+) + \\ & \exp(-R_{DQ}\tau_m)(C'_+N_+ + C'_-N_-)] + C'_yN_y[\exp(-R_{ZQ}\tau_m) \times \\ & (C'_+N_- + C'_-N_+) - \exp(-R_{DQ}\tau_m)(C'_+N_+ + C'_-N_-)] \quad (2)\end{aligned}$$

This conversion is driven by cross-correlated fluctuations. At the end of the mixing time τ_m, the C'_xN_x and C'_yN_y terms are recorded in two separate experiments using 90° shifts of the phases ϕ_3 and ϕ_4. The ^{15}N magnetization is then allowed to evolve, prior to the transfer to ^{13}C coherence for detection. To obtain C′ singlets, the effects of homonuclear $J(C'C^\alpha)$ couplings are removed via an IPAP scheme during acquisition.[17] Each experiment is carried out twice, with different timings of the two final 180° C^α pulses and different phases of the last 90° C′ pulses. The two subspectra give in-phase and anti-phase doublets, which are added and subtracted to separate the two multiplet components. These are then shifted to the center of the original multiplet by $\pm 1/2J(C'C^\alpha)$ and summed together to obtain a singlet. The ^1H spins are decoupled throughout the entire sequence, while C^α 180° pulses are applied during the mixing time τ_m to suppress undesired scalar couplings and interference effects involving C^α spins. The relative signal intensities of the auto- and cross-correlated experiments

$$\langle 2C'_yN_y\rangle/\langle 2C'_xN_x\rangle = \tanh(\Delta R\tau_m) \quad (3)$$

depend on the difference in rates $\Delta R = 1/2[R_{DQ} - R_{ZQ}]$ that corresponds to differential line-broadening.

Chemical Shift Modulation. Several studies[7,16,18−20] have shown that the difference in rates $\Delta R = 1/2[R_{DQ} - R_{ZQ}]$ can be decomposed into three terms:

$$\Delta R = R^{CSM/CSM} + R^{DD/DD} + R^{CSA/CSA} \quad (4)$$

The $R^{CSM/CSM}$ contribution accounts for fluctuations of isotropic chemical shifts (CS) that affect simultaneously the environments of C′ and N nuclei of the same peptide plane. They are characterized by time-scales that typically fall in the microsecond to millisecond range.[18] These CS fluctuations can be caused by changes of dihedral ψ and ϕ backbone angles, as can be rationalized by *ab initio* calculations.[21] In the case of metal-binding proteins, they can also result from interactions with metal ions. The sign of the $R^{CSM/CSM}$ contribution depends on the signs of the changes of the C′ and N chemical shifts upon conformational exchange. The modulations of the isotropic shifts are said to be correlated or anti-correlated if the $R^{CSM/CSM}$ rates are positive or negative.

The second term in eq 4 comprises contributions from various auto- and cross-correlated dipole−dipole effects.[22] As discussed elsewhere,[10] the contributions to $R^{DD/DD}$ due to various dipolar autorelaxation processes can safely be neglected, and cross-relaxation processes are estimated from the 3D structure. The third term in eq 4 arises from cross-correlated CSA relaxation of C′ and N nuclei due to concerted modulations of the chemical shifts that are caused by molecular motions. A study of cross-correlated relaxation in ubiquitin[23] showed that some of the principal components of the CSA tensors are, to a great extent, independent of the environment, while others are correlated with the isotropic shifts. These empirical correlations were found to be largely independent of the model for the peptide plane motions. Thus, for C′ nuclei in ubiquitin, the σ_{yy} component of the CSA tensor, which is nearly parallel to the C═O bond, turns out to be roughly proportional to the isotropic chemical shift ($\sigma_{yy} = 3\sigma_{iso} - 334.9$ ppm), whereas the other two components are almost invariant ($\sigma_{xx} = 251.2$ ppm and $\sigma_{zz} = 83.6$ ppm). For amide ^{15}N nuclei, one finds that $\sigma_{yy} = 2\sigma_{iso} - 163.2$ ppm, $\sigma_{xx} = \sigma_{iso} + 105.5$ ppm, and $\sigma_{zz} = 57.7$ ppm. Assuming that these empirical rules, originally derived for ubiquitin,[23] are also applicable to the proteins under study, we obtained rough estimates of the site-specific $R^{CSA/CSA}$ contributions and hence determined the "corrected" exchange rates $R^{CSM/CSM}$. Moreover, to get a feeling of the robustness of this approach, we found that a ±10% variation of the CSA tensor components translates into a variation of the $R^{CSA/CSA}$ rates of ca. ±15%. This did not affect the interpretation of the experiments performed in this work. This approach is similar to the analyses of cross-correlated relaxation in Major Urinary Protein (MUP) in the presence or absence of a pheromone[18] and of the human centrin 2 in complex with the target peptide XPC.[10]

Results

Direct ^{13}C Detection. The 75-residue protein calbindin D_{9k} in its calcium-loaded form (Ca_2Cb) was used to test the protonless sequence of Figure 1 (see Experimental Section for details). This protein comprises two EF-hand domains and can bind two Ca^{2+} ions.[24] The assignment, structure, and dynamics of calbindin are well-known.[11,24−26] One of the two calcium ions can be easily replaced by a metal ion of the lanthanide series.[27] Such substitutions lead to systems with similar structures but different spectroscopic properties, depending on

(16) Wist, J.; Perazzolo, C.; Bodenhausen, G. *Appl. Magn. Reson.* **2005**, *29*, 251–259.
(17) Bermel, W.; Bertini, I.; Duma, L.; Emsley, L.; Felli, I. C.; Pierattelli, R.; Vasos, P. R. *Angew. Chem., Int. Ed.* **2005**, *44*, 3089–3092.
(18) Perazzolo, C.; Wist, J.; Loth, K.; Poggi, L.; Homans, S. W.; Bodenhausen, G. *J. Biomol. NMR* **2005**, *33*, 233–242.
(19) Frueh, D. *Prog. NMR Spectrosc.* **2002**, *41*, 305–324.
(20) Dittmer, J.; Bodenhausen, G. *J. Am. Chem. Soc.* **2004**, *126*, 1314–1315.
(21) Arnold, W. D.; Oldfield, E. *J. Am. Chem. Soc.* **2000**, *122*, 12835–12841.
(22) Konrat, R.; Sterk, H. *Chem. Phys. Lett.* **1993**, *203*, 75.
(23) Loth, K.; Pelupessy, P.; Bodenhausen, G. *J. Am. Chem. Soc.* **2005**, *127*, 6062–6068.
(24) Akke, M.; Drakenberg, T.; Chazin, W. J. *Biochemistry* **1992**, *231*, 1011–1020.
(25) Bertini, I.; Donaire, A.; Jiménez, B.; Luchinat, C.; Parigi, G.; Piccioli, M.; Poggi, L. *J. Biomol. NMR* **2001**, *21*, 85–98.
(26) Bertini, I.; Carrano, C. J.; Luchinat, C.; Piccioli, M.; Poggi, L. *Biochemistry* **2002**, *41*, 5104–5111.
(27) Bertini, I.; Lee, Y.-M.; Luchinat, C.; Piccioli, M.; Poggi, L. *ChemBioChem* **2001**, *2*, 550–558.

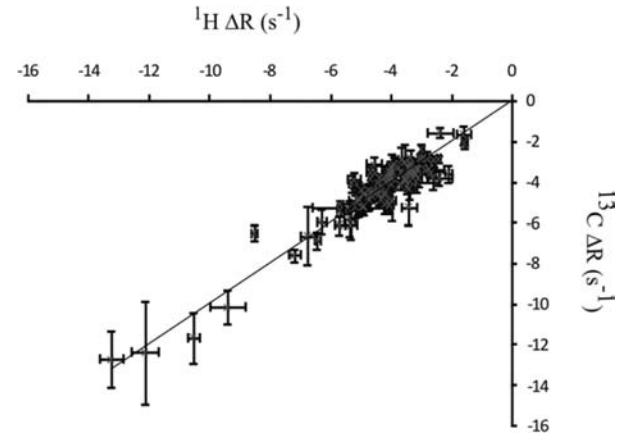

Figure 2. Difference in the relaxation rates $\Delta R(C'N) = 1/2[R_{DQ} - R_{ZQ}]$ of C′N double- and zero-quantum coherences measured either by "protonless" ^{13}C-detected experiments (vertical axis) or via ^{1}H-detected experiments (horizontal axis) for both diamagnetic CaLaCb and paramagnetic CaCeCb. The error bars represent experimental uncertainties in both experiments.

the lanthanide ion.[25,27] Here, we studied diamagnetic La^{3+}- and paramagnetic Ce^{3+}-substituted derivatives (CaLaCb and CaCeCb). For each of these systems, the difference $\Delta R(C'N)$ of the relaxation rates of zero- and double-quantum coherences involving ^{13}C′ and ^{15}N nuclei belonging to the same peptide bond (see Experimental Section) was measured twice, either by traditional HNCO-type experiments (using coherence transfer from and to ^{1}H nuclei) or by protonless ^{13}C-detected CON-type sequences (Figure 1). As shown in Figure 2, the results obtained by the two methods are in good agreement and provide reliable measurements of multiple-quantum relaxation rates $\Delta R(C'N)$.

For the diamagnetic CaLaCb form of calbindin, the $\Delta R(C'N)$ rates of 57 of the 74 amide bonds could be measured with both approaches. Two further rates could be determined only with conventional proton detection, while 6 additional rates could be measured only using protonless experiments, thus giving a total of 65 rates. This shows that the two experiments are complementary. Even in the absence of paramagnetic centers, protonless experiments can provide more rates than proton-detected methods.

In the case of the paramagnetic CaCeCb form of calbindin, there are 9 amide bonds for which the rates $\Delta R(C'N)$ could be determined *only* by protonless experiments and 54 signals that could be detected in both ^{1}H and ^{13}C experiments. This could be expected, as signal losses due to paramagnetic relaxation are more dramatic for protons because of their large gyromagnetic ratios.[28] These observations demonstrate the interest of direct ^{13}C detection.

If one neglects relaxation, ^{1}H-observed experiments should have a sensitivity gain of $(\gamma_H/\gamma_C)^{5/2} = 32$ compared to experiments that start and end with ^{13}C nuclei. However, relaxation is the main cause of intensity losses in our case. Magnetization can be lost through transverse ^{1}H relaxation during the INEPT transfer steps of the HNCO sequence, and even if these fixed delays represent only roughly 20% of the total duration of the sequence, their removal dramatically reduces relaxation losses. Furthermore, INEPT and inverse INEPT steps require a large number of ^{1}H and ^{15}N pulses, which also contribute to signal losses because of pulse imperfections. Coherence transfer steps in protonless ^{13}C-detected experiments

(28) Bertini, I.; Jiménez, B.; Piccioli, M.; Poggi, L. *J. Am. Chem. Soc.* **2005**, *127*, 12216–12217.

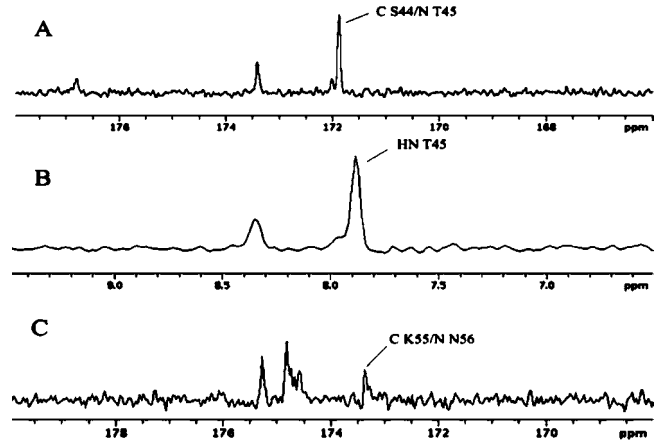

Figure 3. Comparison of the novel "protonless" ^{13}C-detected, and established ^{1}H-detected experiments for paramagnetic CaCeCb at 700 MHz, 298 K, with $\tau_m = 40$ ms. (A) Row corresponding to $i = 44$ (residues S44 and T45) of a protonless ^{13}C-detected CON experiment to measure relaxation of the C'_iN_{i+1} coherence. (B) Matching row ($i + 1 = 45$) of the corresponding ^{1}H-detected HNCO experiment. The ranges of chemical shifts correspond to 12 ppm for ^{13}C and 3 ppm for ^{1}H (both spectral widths are 2.1 kHz.) (C) Signal corresponding to $i = 55$ obtained by the a protonless ^{13}C-detected CON version of the experiment, which could not be observed with the ^{1}H-detected experiment.

are not affected by transverse ^{1}H relaxation, as no proton coherences are involved. This issue is illustrated in Figure 3, which shows selected traces taken from HNCO and CON experiments in diamagnetic CaLaCb and paramagnetic CaCeCb. For diamagnetic systems, the S/N ratio is higher in ^{1}H-detected than in ^{13}C-detected experiments by a factor of about three (Figures 3A,B). In the paramagnetic CaCeCb system, transverse proton relaxation of metal-binding residues can be so fast that the corresponding H^N signals are not visible in the HNCO-type experiment. In contrast, in ^{13}C-detected experiments, $\Delta R(C'N)$ rates can be determined even for metal-bound residues. This is illustrated in Figure 3C for Asn 56, which is close to Ce^{3+}. No such signal can be observed in HNCO-type experiments. Note that the two ways of measuring $\Delta R(C'N)$ rates are complementary, since the dispersion of the signals in C′N 2D spectra is comparable, if not better, than in H^NN spectra.

Slow Backbone Fluctuations in Proteins and Structure−Dynamics Relationships. The above techniques were applied to study slow backbone dynamics of an ensemble of structurally different proteins: calbindin (Cb), Cu,Zn superoxide dismutase (henceforth denoted Cu,Zn SOD), and matrix metalloproteinase 12 (MMP12).

Measured $\Delta R(C'N)$ backbone rates in calbindin are mostly negative, $-13\ s^{-1} < \Delta R(C'N) < -2\ s^{-1}$. Following the procedure described in previous work,[10] $R^{CSM/CSM}$ rates were extracted from the measured $\Delta R(C'N)$ rates. For each sample, the mean rates and their standard deviation were calculated as described in Experimental Section. One thus finds $\langle R^{CSM/CSM}\rangle = -2.39\ s^{-1}$ and $\sigma = 1.28\ s^{-1}$ for CaLaCb. The results reported in Figure 4A show that significant $R^{CSM/CSM}$ contributions exist across the entire backbone of the protein. Using a terminology introduced previously,[7,10,16,18] these negative $R^{CSM/CSM}$ rates indicate that mostly anti-correlated modulations are observed throughout the calbindin backbone. In addition, significant deviations of $R^{CSM/CSM}$ rates from their average occur for 16 residues. Remarkably, 14 out of the 16 outlying residues are located in the calcium-binding loops I and II, in the linker region, and in the C- and N-terminal ends. Moreover, EF-hand loops I (residues

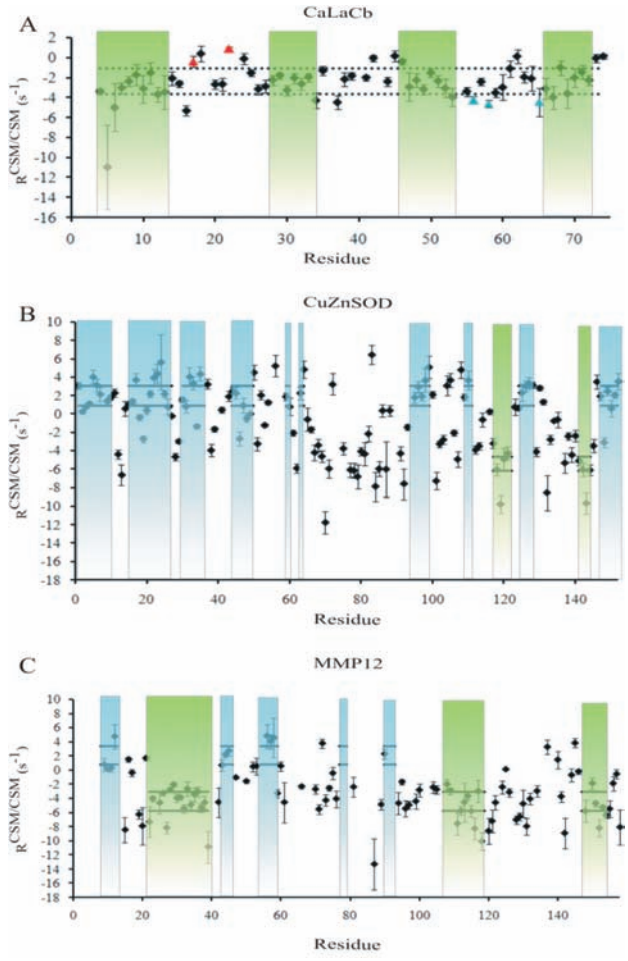

Figure 4. $R^{CSM/CSM}$ rates obtained for the proteins (A) CaLaCb, (B) Cu,Zn SOD, and (C) MMP12. Background colors refer to the secondary structures: green for α-helices and blue for β-sheets. In CaLaCb, local deviations of $R^{CSM/CSM}$ from the average are observed in the two metal binding loops. Residues that coordinate the metal ion in loops I (residues 17 and 22) and II (residues 56, 58, and 65) are highlighted in red and blue, depending on whether metal binding occurs through the backbone carbonyl oxygen or through side chain carboxylate groups. For CaLaCb, dashed lines indicate the standard deviations with respect to the average $\langle R^{CSM/CSM}\rangle$ of the entire protein. For Cu,Zn SOD and MMP12 (panels B and C), the dashed lines denote *local* averages and standard deviations for individual secondary structure elements (α-helices and β-sheets). The numbers of the amino acids refer to the carbonyl atoms, i.e., $i = 54$ correspond to double- and zero-quantum coherences involving C′($i = 54$) and N($i = 55$).

14−27) and II (residues 54−65) feature different behaviors. In loop I, deviations $|R^{CSM/CSM} - \langle R^{CSM/CSM}\rangle|$ that are much larger than the standard deviation are observed for five residues (Lys16, Glu17, Gly18, Gln22, Ser24), indicating more pronounced exchange contributions. As shown in Figure 4A, four of the $R^{CSM/CSM}$ rates are smaller (i.e., less negative) and one is larger (more negative). Alternatively, among the three residues in loop II (Asn56, Asp58, Ser62) that have $R^{CSM/CSM}$ rates that deviate from the average, two (Asn56 and Asp58) have rates that are larger in magnitude (more negative). In addition, Glu65 also appears to exhibit a lower rate, although our criteria led us to discard it from further analysis. Interestingly, the $R^{CSM/CSM}$ rates of Glu17 and Gln22 in binding loop I, which bind the metal ion via their backbone carbonyl oxygens, lie above the average (depicted in red in Figure 4A). The $R^{CSM/CSM}$ rates of Asn56 and Asp58 in loop II (shown in blue in Figure 4A), which bind the metal ion via their side chain carboxylate groups, have the largest (most negative) rates. These findings show that exchange in calbindin, as reflected in the values of the $R^{CSM/CSM}$ rates, increases in binding loops and suggest that the correlation or anti-correlation of the chemical shift fluctuations of the $^{13}C'$ and ^{15}N nuclei may be related to the way residues are bound to the metal, namely, *via* backbone carbonyl groups (loop I) or *via* side chain carboxylate groups (loop II). Significant deviations of the $R^{CSM/CSM}$ rates from their average were also observed in the linker region (Pro37, Gly42, Thr45), as well as in the C- and N-terminal ends. Incidentally, a comparison of the $R^{CSM/CSM}$ rates obtained either by assuming that $S^2 = 1$ or by using the $S^2 < 1$ determined by ^{15}N single quantum measurements gives consistent results, except for residue Gly42. This could be explained by the presence of internal motions in the subnanosecond time scale that are known from ^{15}N relaxation measurements[11] to take place in the linker region and centered around Gly42. The calculated dipole−dipole and CSA/CSA contributions may not be reliable for very flexible residues. Nevertheless, the observed $R^{CSM/CSM}$ rates allowed us to identify significant exchange contributions, most of which could not be detected before. This confirms the ability of backbone C′N coherences to reveal fluctuations of the backbone structure through complementary ^{13}C direct and ^{1}H indirect detection methods. These results corroborate previous observations[10,18] that proteins may undergo conformational exchange across their entire backbone. The presence of increased exchange in more loosely structured regions such as loops and linkers raises the possibility of a relationship between secondary structure elements and dynamics in the μs-ms time scale. This point was further investigated by measuring $R^{CSM/CSM}$ rates in Cu,Zn SOD and MMP12 by protonless direct ^{13}C detection.

The protein Cu,Zn SOD (PDB entry 2K4W) is a monomeric 154-amino-acid enzyme, isolated from *Salmonella enterica*,[29] and comprises an eight-stranded greek-key β-barrel, two small α-helices, and a loop region stabilized by a Zn^{2+} ion. The enzymatic cavity is defined by an electrostatic loop, which contains a copper ion that can jump between oxidation states $Cu^{2+/+}$ and is responsible for the catalytic activity. The three-dimensional structure of this enzyme has been determined in solution,[14] and the complete NMR assignment is available.[30] Crystal structures of many homologous enzymes are also available.[31]

The $R^{CSM/CSM}$ rates obtained for Cu,Zn SOD are shown in Figure 4B. The average trimmed rate (see Experimental Section) was $\langle R^{CSM/CSM}\rangle = -0.86\ s^{-1}$ with a standard deviation $\sigma = 3.69\ s^{-1}$. The rates are scattered across a wide range. There is a clear-cut correlation between the rates obtained from the experiments and the secondary structure (Figure 4B). Indeed, for the 57 residues located in β-sheets, one finds $\langle R^{CSM/CSM}\rangle_\beta = +1.94 \pm 1.90\ s^{-1}$, whereas the average rate observed for the 9 residues in the short α-helices is $\langle R^{CSM/CSM}\rangle_\alpha = -6.13 \pm 2.24\ s^{-1}$. In the loop regions the average rate is $\langle R^{CSM/CSM}\rangle_l = -2.16 \pm 3.71\ s^{-1}$. Therefore, in the β-barrel regions of Cu,Zn SOD, the $R^{CSM/CSM}$ rates are positive and lie in the range $0 < R^{CSM/CSM} < +4\ s^{-1}$, whereas they are negative in the α-helical fragment. We shall see below that the positive rates $R^{CSM/CSM}$ typical of β-sheets are characteristic of correlated fluctuations of chemical

(29) Gabbianelli, R.; D'Orazio, M.; Pacello, F.; O'Neill, P.; Nicolini, L.; Rotilio, G.; Battistoni, A. *Biol. Chem.* **2004**, *385*, 749–754.
(30) Jiménez, B.; Mori, M.; Battistoni, A.; Sette, M.; Piccioli, M. *Biomol. NMR Assignments* **2007**, *1*, 65–68.
(31) Pesce, A.; Capasso, C.; Battistoni, A.; Folcarelli, S.; Rotilio, G.; Desideri, A.; Bolognesi, M. *J. Mol. Biol.* **1997**, *274*, 408–420.

shifts, while the negative rates found for α-helices reveal anti-correlated fluctuations. In loop regions, the $R^{CSM/CSM}$ rates are intermediate between those measured in α-helices and β-barrels and characterized by standard deviations larger than those observed in well-defined secondary structure elements.

Further evidence of a relationship between secondary structure elements and $R^{CSM/CSM}$ rates was provided by experiments performed on MMP12 (Figure 4C). Matrix metalloproteinases are composed of a catalytic domain and a hemopexin-like domain.[32] The catalytic domain adopts a typical MMP fold and binds one "structural" Zn^{2+} ion as well as three Ca^{2+} ions, in addition to the catalytic Zn^{2+} ion.[33] The 3D fold is composed of five β-sheets flanked by the Zn^{2+} binding loop, and two long α-helices that also include the active site. The C-terminal region comprises a long loop and a small α-helix. Structures determined by solution NMR[34] and by X-ray diffraction[35] (PDB entries 1Y93 and 1RMZ) of this protein are available. As this enzyme contains both α-helices and β-sheets, it seemed an appropriate system to complement our observations on the α-helices of calbindin and the β barrel protein Cu,Zn SOD.

The average $R^{CSM/CSM}$ rates calculated for each secondary structure in MMP12 indicate a similar pattern and therefore corroborate our previous observations. Indeed, the β-sheet features correlated motions, with $\langle R^{CSM/CSM}\rangle_\beta = +2.46 \pm 1.85$ s^{-1}, whereas the α-helices show anti-correlated CSM motions with $\langle R^{CSM/CSM}\rangle_\alpha = -5.04 \pm 2.29$ s^{-1}. Finally, as in the cases of calbindin and Cu,Zn SOD, the behavior of loop regions is characterized by negative $R^{CSM/CSM}$ rates with a much larger scatter $\langle R^{CSM/CSM}\rangle_l = -3.24 \pm 3.49$ s^{-1}.

Discussion

The three proteins studied in this work have very different properties, in terms of secondary structures, three-dimensional folds, biological function, and NMR relaxation rates. Nevertheless, our observations reveal a relationship between secondary structure elements and $R^{CSM/CSM}$ rates. The evidence shows that β-sheets and α-helices are associated with correlated and anti-correlated chemical shift modulations. This relationship is striking when representing $R^{CSM/CSM}$ rates against backbone Ψ angles for the three proteins (Figure 5). The range $\Psi = -45° \pm 25°$, typical of α-helical structures, corresponds to negative $R^{CSM/CSM}$ rates. Angles in the range $\Psi = +140° \pm 30°$ are characteristic of β-sheets and correspond to positive $R^{CSM/CSM}$ rates. The empirical relationship between $R^{CSM/CSM}$ rates and the type of secondary structure element thus turns out to be a general feature. The contribution to multiple quantum relaxation rates of C′N coherences due to chemical shift modulations arising from fast two-site exchange is given by[19,36]

$$R^{CSM/CSM} = 2p_a p_b \tau_{ex} \Delta\omega_{C'} \Delta\omega_N \qquad (5)$$

where $\tau_{ex} = 1/(k_{AB} + k_{BA})$, $\Delta\omega_{C'}$ and $\Delta\omega_N$ are the changes of the isotropic chemical shifts experienced by C′ and N nuclei when hopping from one site to another, and p_a and p_b are the populations of the two conformations.[7] The sign of the rate $R^{CSM/CSM}$ depends on the relative signs of $\Delta\omega_{C'}$ and $\Delta\omega_N$. Therefore, valuable insight can be gained by correlating chemical shift *variations* with specific secondary structure elements. To our knowledge, only relationships between "static" C′ and N chemical shifts (as opposed to chemical shift *modulations*) and backbone secondary structure have been addressed so far.[36] It is clear that backbone motions, i.e., modulations of ϕ, ψ angles accompanied by the making and breaking of hydrogen bonds, should induce modulations of isotropic chemical shifts. To rationalize our observations, one needs information not only about the dihedral angles that are affected by the dynamic processes but also about the relationship between structures and chemical shifts. Many different factors, such as hydrogen bonding, backbone conformation, and side chain conformation of neighboring residues, contribute to ^{15}N chemical shifts in proteins.[37] Backbone ^{13}C chemical shifts are apparently more sensitive to side chain conformations than to the neighboring residues.[38]

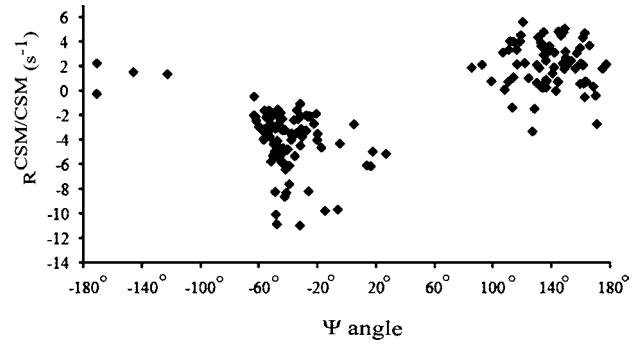

Figure 5. Overview of all $R^{CSM/CSM}$ rates determined in CaLaCb, Cu,Zn SOD, and MMP12, plotted as a function of the backbone dihedral angle ψ. The clusters to the left and right correspond to α-helices and β-sheets.

A recent model developed by Wingreen and co-workers aims at predicting characteristic motions in helices and sheets.[39,40] According to these authors a generic β-sheet undergoes twisting or bending about an axis located in the plane of the sheet. In this case, the different strands that constitute the sheet should undergo displacements with respect to one another, without deformations of the strands themselves, therefore leaving all backbone ψ angles unchanged. On the other hand, interstrand distances are modulated during this kind of motion, so that a weakening of hydrogen bonds should be expected. Density functional theory (DFT) calculations by Xu and Case[38] predict variations of ^{15}N and ^{13}C chemical shifts in model peptides that adopt β-sheet conformations. Their predictions show that both amide ^{15}N and carbonyl ^{13}C chemical shifts move to higher frequencies when going from an isolated β-strand to the central strand of a triple-stranded β-sheet, due to modifications of hydrogen bond patterns and strengths. This would lead to a positive product $\Delta\omega_{C'}\Delta\omega_N$ and therefore to a positive $R^{CSM/CSM}$ rate, in agreement with our observations. For double-stranded sheets, the calculated ^{13}C chemical shifts differences are again positive but small compared to the single-strand configuration,

(32) Johnson, L. L.; Dyer, R.; Hupe, D. J. *Curr. Opin. Chem. Biol.* **1998**, *2*, 466–471.
(33) Bode, W.; Fernandez-Catalan, C.; Tschesche, H.; Grams, F.; Nagase, H.; Maskos, K. *Cell. Mol. Life Sci.* **1999**, *55*, 639–652.
(34) Bertini, I.; Calderone, V.; Cosenza, M.; Fragai, M.; Lee, Y.-M.; Luchinat, C.; Mangani, S.; Terni, B.; Turano, P. *Proc. Natl. Acad. Sci. U.S.A.* **2005**, *102*, 5334–5339.
(35) Bertini, I.; Calderone, V.; Fragai, M.; Luchinat, C.; Mangani, S.; Terni, B. *Angew. Chem., Int. Ed.* **2003**, *42*, 2673–2676.
(36) Wishart, D. S.; Case, D. A. *Methods Enzymol.* **2001**, *338*, 3–34.
(37) Oldfield, E. *Annu. Rev. Phys. Chem.* **2002**, *53*, 349–378.
(38) Xu, X. P.; Case, D. A. *Biopolymers* **2002**, *65*, 408–423.
(39) Emberly, E. G.; Mukhopadhyay, R.; Tang, C.; Wingreen, N. S. *Proteins* **2004**, *55*, 91–98.
(40) Emberly, E. G.; Mukhopadhyay, R.; Wingreen, N. S.; Tang, C. *J. Mol. Biol.* **2003**, *327*, 229–237.

although they may lead to small negative $R^{CSM/CSM}$ rates.[38] This could explain some of the weak negative contributions to $R^{CSM/CSM}$ observed in β-sheets.

In our observations in three proteins, 91 residues are located in β-strands. Among them, 69 are associated with positive $R^{CSM/CSM}$, in accordance with the above line of reasoning, whereas for 13 residues the CSM rates could not be measured. The remaining 9 residues have negative $R^{CSM/CSM}$ rates, 8 of which were observed in Cu,Zn SOD. These rates need to be analyzed on the basis of the Cu,Zn SOD structure and confronted with our hypothesis. The corresponding residues are Ser18, Ile19, Thr27, Thr34, Gly46, His48, Asp93, and Tyr148. Ser18 and His48 have rates $R^{CSM/CSM} = -0.37 \pm 0.38$ and -0.49 ± 0.51 s^{-1}. Considering the experimental errors, these rates are not significantly negative. Gly46 belongs to the β-strand 44−50, which is flanked by the β-sheet 124−128. The partner residue of Gly46 in this strand is His128, which is situated at the end of the β-sheet at the transition to the nearby loop, so that the hydrogen bond pattern is disrupted in the case of Gly46. Therefore, basing our interpretation on the model calculations of Xu and Case,[38] one should not expect clearly positive $R^{CSM/CSM}$ rates. The same reasoning can be applied to Thr34. Residues Thr27 and Asp93 are located at the end of a β-strand and therefore fall into the same category. Finally, Ile19 and Tyr148 have unusual ψ angles, which may explain the negative $R^{CSM/CSM}$ rates. In the case of MMP12, the residue Ala60, which is located at the end of a β-strand, is also associated with a negative $R^{CSM/CSM}$ rate.

According to the description of Wingreen and co-workers, the main motional modes in α-helices consist of bending and twisting motions about the average helix axis.[40] Such motions imply the occurrence of fluctuations of backbone ψ angles. The ^{15}N chemical shifts depend in a complex manner not only on the dihedral angles $\psi(i-1)$, $\phi(i)$, and $\psi(i)$ of the backbone but also on the dihedral angle $\chi_1(i)$ of the side chain. The ^{15}N chemical shifts are also sensitive to the side chain dihedral angle $\chi_1(i-1)$ of the preceding residue through the nearest neighbor effect[41] and furthermore affected by hydrogen bonding.[38,41] On the other hand, carbonyl ^{13}C chemical shifts are mainly sensitive to backbone torsion angles $\psi(i)$ and $\phi(i+1)$[43] and therefore give reliable reports on secondary structure. Finally, the average backbone chemical shifts in α-helices were found to be +1.7 ppm for ^{13}C and −1.7 ppm for ^{15}N nuclei with respect to random coil.[44] A transient deformation of a helical region toward a random-coil-like conformation should therefore be associated with $\Delta\omega_{C'}\Delta\omega_N < 0$. This is consistent with our experimental data, which show mostly negative $R^{CSM/CSM}$ rates in helical regions of the proteins.

Concluding Remarks

An unexpected relationship was found to exist between slow conformational backbone dynamics and secondary structure elements in proteins. Slow backbone dynamics were identified through relaxation rates $R^{CSM/CSM}$ of C′N multiple quantum coherences. These rates provide more information than longitudinal and transverse relaxation rates of isolated ^{15}N nuclei, since the $R^{CSM/CSM}$ rates depend on the rates of interconversion between the conformations, on their populations, and on their ^{15}N and ^{13}C chemical shifts. Direct ^{13}C detection of $R^{CSM/CSM}$ rates proved to be valuable for both diamagnetic and paramagnetic proteins. Measurements of $R^{CSM/CSM}$ rates on three different folded proteins revealed the existence of extensive conformational exchange across the entire protein backbones. The relaxation rates of C′N coherences arising from slow backbone dynamics have positive signs (characteristic of correlated fluctuations of the chemical shifts of neighboring ^{15}N and ^{13}C nuclei) in β-sheets and negative signs (characteristic of anticorrelated shift fluctuations) in α-helices. These observations extend the prospect of structure−dynamics relationships to time scales on which protein function and enzymatic activity actually take place. In our view, this represents a significant step toward the development of functional dynamics.

Acknowledgment. We thank Marco Fragai (CERM, University of Florence), Andrea Battistoni, and Marco Sette (University of Rome "Tor Vergata") for providing doubly labeled samples of MMP12 and Cu,Zn-SOD. This work was supported by the European Commission ("European Network of Research Infrastructures for providing Access and Technological Advancements in bio-NMR", EUNMR Contract No. RII3-026145).

Supporting Information Available: All $R^{CSM/CSM}$ rates. This material is available free of charge via the Internet at http://pubs.acs.org.

JA9103556

(41) Le, H.; Oldfield, E. *J. Phys. Chem.* **1996**, *100*, 16423–16428.
(42) Le, H.; Oldfield, E. *J Biomol NMR* **1994**, *4*, 341–348.
(43) Wishart, D. S.; Case, D. A. *Methods Enzymol.* **2001**, *338*, 3–34.
(44) Wishart, D. S.; Sykes, B. D. *Methods Enzymol.* **1994**, *239*, 363–392.